

# On the Selection of the Current Collector for Water Processed Activated Carbon Electrodes for Their Application in Electrochemical Capacitors

Paulo Luís,<sup>[a]</sup> Silvia Martin-Fuentes,<sup>[a]</sup> María Arnaiz,\*<sup>[a]</sup> and Jon Ajuria\*<sup>[a]</sup>

Electrode manufacturing for electrochemical energy storage technologies often relies on hazardous fluorine-containing compounds and toxic organic solvents. To align with sustainability goals and reduce costs, there is a pressing need for water-processable alternatives. These alternatives can halve electrode processing costs and ease regulatory burdens. While progress has been made with water-processed graphite electrodes using eco-friendly binders, challenges persist for high-mass loading activated carbon (AC) electrodes. This study investigates the impact of modified aluminium current collectors on water-processed AC electrodes, focusing on compatibility, processability, and electrochemical performance. Various aluminium foils, including etched and carbon-coated types, were evaluated. The results show that modifications at the interface

significantly improve the wetting properties and mechanical stability. Electrochemical tests revealed that carbon-coated aluminium provided the lowest internal resistance and highest rate capability due to intimate contact between the electrode components. In contrast, etched aluminium foil exhibited higher contact resistance and poorer performance. Ageing studies demonstrated that carbon-coated foils maintained better electrochemical performance over time, as the carbon layer reduced degradation reactions and contact resistance. These findings suggest that uniformly carbon-coated aluminium current collectors are the optimal choice for high-power electrochemical capacitors, balancing performance, sustainability, and cost-efficiency.

## 1. Introduction

As the world transitions towards a greener and more sustainable society, the importance of electrochemical energy storage becomes increasingly evident. In parallel, rapid advancement of more sophisticated portable electronics and electrical vehicles has elevated the requirements for electrochemical energy storage systems, specifically in terms of high-energy and high-power densities, prolonged lifespan and reduced costs. Among the available technologies, the market is currently dominated by lithium-ion batteries (LIBs), owing to their high energy densities, despite having low power performances and limited lifespan, ascribed to the faradaic nature of the charge storage mechanism. Moreover, LIBs rely on critical raw materials (CRM),<sup>[1]</sup> fueling the need to explore more powerful and sustainable alternative technologies. Electric double-layer capacitors (EDLCs), entirely rely on activated carbon (AC), being a

CRM-free technology governed through the adsorption/desorption of ions in the electrolyte at the electrode surface, exhibiting long lifespan and operating at high specific powers. However, the energy density falls far behind LIBs, limiting their widespread. To address the complementary energy-power features of the two technologies, an effective strategy involves the construction of metal-ion capacitors (MICs) such as lithium-ion capacitors (LICs), combining a high-power capacitive positive electrode (e.g., AC) and a high-energy faradaic negative electrode (e.g. graphite, hard carbon, ...).<sup>[2]</sup> LICs, a technology that reached the market presenting higher energy than EDLCs while being only based on carbonaceous materials, still share the use of graphite in the negative electrode, whose shortfall is expected to slow-down the widespread of electric vehicles adoption. Sodium can be a solution in this technological scenario. It is not only an abundant earth resource but also possesses physical and electrochemical similarities with its lithium counterpart, prompting the research and development of sodium-ion energy storage technologies,<sup>[3]</sup> e.g. sodium-ion batteries (SIB) and capacitors (SICs), enabling more sustainable technologies. Despite the many differences of the above-mentioned technologies in terms of materials and performance, they share common traditional electrode manufacturing processes, based on the use of health-hazardous fluorine-containing compounds, such as polytetrafluoroethylene (PTFE) or polyvinylidene difluoride (PVdF) binders, with the latest dispersed in toxic organic solvents, like N-methyl-2-pyrrolidone (NMP).<sup>[4]</sup> Therefore, in alignment with the green premises and for the sake of sustainability, water-processable slurries are in high demand in order to substitute toxic compounds that require

[a] P. Luís, S. Martin-Fuentes, M. Arnaiz, J. Ajuria

Centre for Cooperative Research on Alternative Energies (CIC energiGUNE), Basque Research and Technology Alliance (BRTA), Alava Technology Park, Albert Einstein 48, Vitoria-Gasteiz 01510, Spain

E-mail: marnaiz@cicenergigune.com

jajuria@cicenergigune.com

 Supporting information for this article is available on the WWW under <https://doi.org/10.1002/batt.202400405>

 © 2024 The Authors. *Batteries & Supercaps* published by Wiley-VCH GmbH. This is an open access article under the terms of the Creative Commons Attribution Non-Commercial NoDerivs License, which permits use and distribution in any medium, provided the original work is properly cited, the use is non-commercial and no modifications or adaptations are made.

complex and cost increasing waste treatment solutions. Additionally, a shift towards water-based dispersions would not only be beneficial from an economic point of view, halving the electrode processing costs, but also in terms of regulatory relief, enabling further proliferation of the technology.<sup>[5]</sup> Great progress has been achieved on processing water-based graphite and HC electrodes containing more environmentally friendly carboxymethyl cellulose (CMC) and styrene butadiene rubber (SBR) binders, reaching high mass loading requirements demanded by manufacturers.<sup>[6]</sup> On the other hand, water-based processing remains a challenge for AC when reaching high mass loadings with research ongoing for new binders and formulations that enable the fabrication of high mass loading electrodes.<sup>[7–9]</sup> In light with the improvements needed to address the technological sustainability, a high energy density EDLC with 5000 F employing water-processable binders has been reported,<sup>[10]</sup> evidencing a significant gain in momentum. On the other hand, cost reduction is required to aid the integration of the technology in the market. For instance, the current collector, representing 17% of the final cost of an EDLC, ought to receive more attention since it impacts the processability and ultimately the performance on the technology.<sup>[11]</sup> It plays a pivotal role in the architecture of electrochemical energy storing electrodes since it acts as the bridge between the electrochemical storing device and the external circuit, as well as the supporting substrate to harbor the active electrode material. Consequently, the current collector influences the storing and rate capabilities, heat transfer properties and long-term stability.<sup>[12,13]</sup> Accordingly, special attention is required when selecting a suitable current collector for high-power storing technologies. For instance, EDLCs rely on the use of aluminium current collectors. However, the scenario is different with regard to metal-ion capacitors. While LICs require in the negative electrode the use of copper current collectors to avoid alloying of lithium with aluminium at low potentials, SICs can use aluminium current collector since sodium avoids such alloying process. Thus, the replacement of copper with aluminium carries a multitude of additional benefits, such as its vast abundance, decreasing the overall cost of the technology. Moreover, aluminium possesses lower density compared to copper, allowing the construction of lighter electrochemical architectures with enhanced specific energy densities.<sup>[14]</sup>

In order to achieve high efficiency and stable operation, the selection of a current collector follows a number of criteria, focusing on i) high electrical conductivity and low contact resistance with the coating, ii) electrochemical stability, iii) mechanical strength, iv) optimal density, v) sustainability and vi) cost.<sup>[15]</sup> Typically, a metallic current collector foil possesses limited contact area and weak adhesive properties towards the coating, inherently related to the smooth surface, which results in a high contact resistance. Previous studies concluded that the contact resistance occupies a significant portion of the total impedance, hence, an intimate physical contact between the coating and the current collector is paramount to reduce the internal resistance of the cell.<sup>[16,17]</sup> In this regard, reinforcing the physical contact between the conductive components leads to the reduction of the internal resistance of the device. Addition-

ally, through adequate modification of the density and strength, higher volumetric energy densities can be achieved by stacking more active material in a finite space. Bestowing novel functionalities through the modification of the current collector can further improve the overall properties and are categorized in 3D-engineered conductive substrates or with added-multi-functionality through coating. Through carefully controlled physicochemical processes, foam,<sup>[18]</sup> etched,<sup>[19,20]</sup> nanostructure-grown<sup>[21]</sup> and laser patterned<sup>[22–25]</sup> current collectors can be produced and fall under the first category. On the other hand, priming<sup>[26–32]</sup> and metallization of fibrous substrates<sup>[33]</sup> encompass the last classification. Although impressive results were vastly reported in the literature, these might find difficulties reaching the market due to the complicated, costly, and time-consuming processes. Accordingly, other options should be considered, matching the requirements for the mass production of electrochemical capacitors.

In this work, it is studied the impact of some modified aluminium current collectors available in the market, specifically one etched and two carbon-coated foils. The research was focused on water-processed activated carbon electrodes considering the challenges these represent in securing high mass loadings due to their high specific surface area (*i.e.*, ~1700 m<sup>2</sup> g<sup>-1</sup>), and hence, low bulk density (*i.e.*, ~0.30 g cm<sup>-3</sup>). First, compatibility, processability and mechanical stability of water-processed AC electrodes were studied to understand the impact imposed by the modifications at the interface of the aluminium foils. Second, the electrochemical performance of the fabricated electrodes was investigated through the analysis of the internal resistance and rate capability, critical parameters in the development of high-power electrochemical capacitors. Parallelly, the electrodes were also tested in Li- and Na-ion chemistries in order to prove their transversality to MIC technology. Finally, ageing studies were performed by monitoring the evolution of the capacitance and internal resistance in order to identify the most durable modified current collector, while post-mortem microstructural investigations at the interface between the current collector and the coated materials would provide details about the degradation mechanisms taking place.

## Experimental Section

### Current Collectors

Four aluminium foils were selected, specifically a standard bare aluminium (Bare), an etched aluminium foil (E1-CC), and two different carbon-coated aluminium foils, (C1-CC and C2-CC). In Table 1 are reported the specifications of those aluminium current collectors.

### Materials

The materials employed throughout the study were purchased from different sources. Carboxymethyl cellulose (CMC, average Mw 700,000, degree of substitution 0.7) and polytetrafluoroethylene (PTFE) in 60 wt% aqueous solution were acquired from Merck KGaA

**Table 1.** Specifications of investigated aluminium current collectors.

Specifications	Bare	E1-CC	C1-CC	C2-CC
Mass loading/mg cm <sup>-2</sup>	5.31	5.08	4.05	4.18
Thickness/ $\mu\text{m}$	20	20	12	15
Density/g cm <sup>-3</sup>	2.65	2.54	3.37	2.77

(Germany). Styrene-butadiene rubber (SBR) 40 wt % water emulsion was obtained from Zeon Corporation (Japan). Conductive carbon additive (C-ENERGY™ Super C45) was purchased from IMERYS (Germany) and the activated carbon (AC, type YP-50 F) from Kuraray Corporation (Republic of Korea). Analytical grade deionized water was obtained from a Wasserlab purification water system (Spain), with a stable conductivity of  $10.0 \mu\text{S cm}^{-1}$ . The main electrolytes comprise 1 M TEABF<sub>4</sub> in acetonitrile (ACN), additionally, 1 M NaPF<sub>6</sub> in 1:1 (v/v) mixture of ethylene carbonate (EC) and propylene carbonate (PC) and 1 M LiPF<sub>6</sub> in 1:1 (v/v) mixture of ethylene carbonate (EC) and dimethyl carbonate (DMC) were used as received from E-lyte (Germany) and Solvionic (France), respectively. For the assembly of modified Swagelok™-type cells, D-type glass microfiber punched filters from Whatman™-Cytiva were used as separators. Sodium or lithium metal used as reference electrode when assembling three electrode cells. In pouch cell configuration, cellulose paper TF40-30 (Nippon Kodashi Corporation, Japan) was employed.

### Slurry and Electrode Fabrication

The slurry comprises AC, conductive carbon additive, and as binders CMC and SBR, all mixed and dispersed in deionized water. Both AC and conductive carbon additive were dried overnight at 120 °C in a dynamic vacuum oven (Memmert GmbH, Germany) before the mixing process. For the mixing and dispersion of the slurry components a disperser-homogenizer (Dissolver DISPERMAT, VMA Getzman), coupled with a chilling unit, in order to maintain a constant temperature of 20 °C throughout the process, was used. Single-side coated electrodes were casted on the different aluminium foils with a K Paint Applicator (RK PrintCoat Instruments Ltd, United Kingdom) at a fixed wet film thickness with a Dr. Blade at a constant speed of  $4.5 \text{ cm s}^{-1}$ . After the casting process, the laminates were partially dried at room temperature for 2.0 hours before drying at 80 °C overnight.

### Lab-scale Cell Assembly

The electrodes were tested in full and half-cell configurations using a two-electrode and three-electrode Swagelok™-type cell. Full cells followed a symmetric EDLC configuration, with a 1.1:1 mass ratio between the positive and negative electrodes. In half-cell, the AC electrodes were employed as working electrodes, with a lithium or sodium metal disc used as reference electrodes and an in-house fabricated oversized self-standing AC as counter electrode. The 12 mm diameter ( $1.13 \text{ cm}^2$ ) electrodes were punched from the laminates using a handheld electrode puncher (Nogamigiken Co., Ltd, Japan) and vacuum-dried at 150 °C overnight in a Büchi glass oven B-585 connected to a vacuum pump V-700 (Büchi, Switzerland) prior to cell assembly to eliminate any moisture. The sandwiched electrodes were interlayered by two 13 mm diameter glass microfiber separators soaked in 1 M TEABF<sub>4</sub> in acetonitrile (ACN) in the case of EDLCs and 1 M LiPF<sub>6</sub> in 1:1 (v/v) (EC:DMC) or 1 M NaPF<sub>6</sub> in 1:1 (v/v) (EC:PC) when tested in Li- or Na-ion chemistries, respectively. The assembly was carried in a glove box

(MBraun, Germany) with oxygen and moisture contents below 0.1 ppm.

### Pouch Cell Fabrication

Monolayer 20 cm<sup>2</sup> pouch cells were assembled to investigate the electrochemical properties. Prior to aluminium tab welding, the electrodes were wrapped with separator. Then, the cell was partially sealed inside an aluminium-coated polymer film and vacuum dried overnight at 150 °C. Finally, 1 M TEABF<sub>4</sub> (ACN) was vacuum impregnated followed by thermal sealing. In order to evaluate the potential evolution of gas during electrochemical activity, an empty area was kept in the pouch cells.

### Material Characterization

In order to evaluate the rheological properties of the slurry, the viscosity was analyzed at a shear rate range of 0.1 and  $1000 \text{ s}^{-1}$  in a rotational rheometer (HAAKE™ Rheostress™ ThermoFisher Scientific), employing a 60 mm/1° cone-type sensor. Scanning electron microscopy (SEM) was used to investigate the surface and cross sectioned morphology of the current collectors and activated carbon electrodes. Micrographs were obtained from a Thermo Fisher Quanta 200 FEG high resolution scanning electron microscope (Thermo Fisher Scientific, United States of America). Cross sections were performed with a Hitachi 4000 Plus ion mill, equipped with a broad, low-energy Ar<sup>+</sup> ion beam (0–6 kV acceleration voltage) milling process. To investigate the cohesion of the coatings and the adhesive properties of the electrode on the different current collectors, peel test measurements were carried out in a Instron 34SC-5 single column table model (Illinois Tool Works Inc., United States of America). The bulk resistivity of the laminates was obtained using a multipoint probe system (RM2610, HIOKI Corp., Japan) at room temperature. Contact angle measurements were performed on the aluminium current collector foils using a tensiometer LSA 100 Surface Analyzer (Lauda Scientific, Germany). All measurements were conducted at room temperature. X-ray diffraction (XRD) patterns were registered for pristine and aged aluminium samples in a Bruker D8 X-ray diffractometer, with data collection at 40 kV and 40 mA employing CuK $\alpha$  radiation over 20 within the range 10–80° at steps of 0.02° and a residence time of 5 s. Solution nuclear magnetic resonance (NMR) experiments were performed to determine any by-product generated in the electrolyte during the aging tests. NMR spectra were collected at 300 K on a 300 Bruker AVANCE III HD spectrometer equipped with a Bruker BBFO z-gradient 5 mm BBFO probe head. The nuclei under study were <sup>19</sup>F and <sup>27</sup>Al and data were analyzed with Topspin software.

### Electrochemical Characterization

The electrochemical performance of both Swagelok™ and pouch cells were assessed using a multichannel potentiostat VMP3 and BT-Lab (Biologic, France), respectively. Cyclic voltammetry (CV), galvanostatic charge-discharge (GCD) and electrochemical impedance spectroscopy (EIS) were selected to evaluate the cells. All measurements were carried out at room temperature.

In half-cells, the potential window was limited between 2.0 and 4.0 V vs. Li<sup>+</sup>/Li or Na<sup>+</sup>/Na, while in full cells the cell voltage was set between 0 and 2.7 V. CVs were carried at scanning rates between 10 and 100 mV s<sup>-1</sup> for 10 cycles, while in GCD the cells were tested at specific current densities ranging from 1 and 50 Ag<sup>-1</sup> for a total of 5 cycles. For all experiments, the last cycle was selected for interpretation and representation of the results.

The areal capacitance ( $C_A$ ) was calculated from the GCD profiles following the equations below.

$$C = i \cdot \frac{t_d}{V_f - V_i} \quad (1)$$

$$C_A = \frac{C}{A} \quad (2)$$

Where  $C$  stands for the capacitance (F),  $i$  is the current (A),  $t_d$  is the discharge time (s),  $V_f$  is the recorded potential after the IR drop (V),  $V_i$  is the minimum voltage (V) and  $A$  is the geometric area of the electrode ( $\text{cm}^2$ ).

The internal resistance  $IR$  ( $\Omega$ ) was calculated from the GCD profiles according to the following equation.

$$IR = \frac{V_{cutoff}^+ - V_f}{i} \quad (3)$$

Where  $V_{cutoff}^+$  is the cutoff potential or upper cell voltage (V) previously selected.

In pouch cells, electrochemical tests were limited by a working cell voltage between 0 and 2.7 V. As in the previous experiments, CVs were performed at a scanning rate ranging between 10 and 100  $\text{mVs}^{-1}$ . GCD was carried out between a current range of 1 and 10 A (6–62  $\text{A g}^{-1}$ ).

Electrochemical impedance spectroscopy was recorded between the frequencies 100 kHz and 10 mHz with 5 mV amplitude at OCP.

Long-term cyclability investigations were carried out in pouch cells by consecutively performing galvanostatic charge-discharge cycles at 5 A, which accounts for a discharge time of 5 seconds, with electrochemical impedance being performed every 5,000 cycles. The electrochemical testing was terminated upon reaching the end-of-life state (*i.e.*, 20% initial capacitance decay, and/or 100% resistance increase).

### Post-Mortem Analysis

Post-mortem investigations covered SEM microtopological and cross-sectional analysis of aged electrodes and current collectors, XRD of aged current collectors and NMR investigation of decomposition products in the electrolyte. Beforehand, the pouch cells were disassembled in an inert atmosphere and the aged positive electrodes were carefully extracted, cut in approximately  $1 \times 1 \text{ cm}^2$  pieces and gently immersed in acetonitrile for a 24-hour period to dissolve remaining electrolytic species. To investigate topological and elemental changes at the modified aluminium current collectors, the coating was carefully removed from the previously washed samples with copious water and rubbed with a cotton bud. Then, the electrodes were transferred and stored in clean vials for further evaluation. With respect to NMR investigations of the electrolyte in aged pouch cells, the remaining acetonitrile was allowed to evaporate from the retrieved separator and later immersed in a vial containing deuterated acetonitrile for a 24-h period. Then, the solution was transferred to an NMR tube for further analysis.

## 2. Results and Discussion

### 2.1. Properties of Aluminium Current Collectors

First and foremost, the selected aluminium current collector foils were investigated in regard to their surface properties by SEM. As reported in Figure 1(a), at low magnifications, bare aluminium foil depicts a smooth surface with grooves; however, at higher magnifications, the surface is populated with randomly distributed micrometer-sized pits, likely due to the fabrication process. Likewise, at high magnifications, E1-CC depicts similarities with the previous bare aluminium foil, however, at higher magnifications the surface morphology can be described as rough, with aluminium grains and high density of etched pits with a wide range of pore sizes no greater than 2  $\mu\text{m}$ . From the analysis of Figure 1(c), with respect to C1-CC, a similar pattern is identifiable at the surface of the foil, also observed in the uncoated aluminium foil. At higher magnification, porous aggregates of spherical nanoparticles are shown, likely carbon black, which partially covers the aluminium foil. On the other hand, as shown in Figure 1(d), C2-CC depicts a densely packed porous coating of conductive carbon, which fully covers the aluminium foil.

Additional analysis was performed to understand the degree of hydrophilicity of the selected aluminium current collectors through the determination of the contact angle on each of them. It is believed that higher degrees of hydrophilicity result in better contact between the slurry and the current collector. As reported in Figure 1(e), bare aluminium foil demonstrates the lowest degree of hydrophilicity from the investigated set, with a contact angle of  $68.3^\circ$ , followed by C1-CC ( $21.1^\circ$ ), E1-CC ( $17.2^\circ$ ), and finally C2-CC, which possesses a receding contact angle due to the absorption of the water drop by the porous carbon coating,<sup>[34]</sup> hence, no contact angle value was attributed. As previously observed, C1-CC possesses a partial coating at the surface of the aluminium foil, hence the intermediate values observed. On the other hand, the value obtained for E1-CC is in agreement since it visibly possesses a rough surface, which results in an increase of hydrophilicity according to Wenzel's equation.<sup>[35]</sup>

It is clear that the modification of aluminium foil through etching or coating with a layer of carbon is effective in increasing the hydrophilicity of the current collector. Consequently, better compatibility between the coating and the current collector could be expected.

### 2.2. Physicochemical Characterization of Electrodes

Further microstructural analysis was carried out to understand the impact of the modified current collectors in the mechanical strength and integrity of the electrode, and the electrode material distribution along the surface of the aluminium foils and at the bulk. Figure 2(a-d) depict cross-sectional micrographs of the laminates, focusing on the coating and at the interface between the current collector and the coating. At the microscale, homogeneously dispersed stacked AC with particle

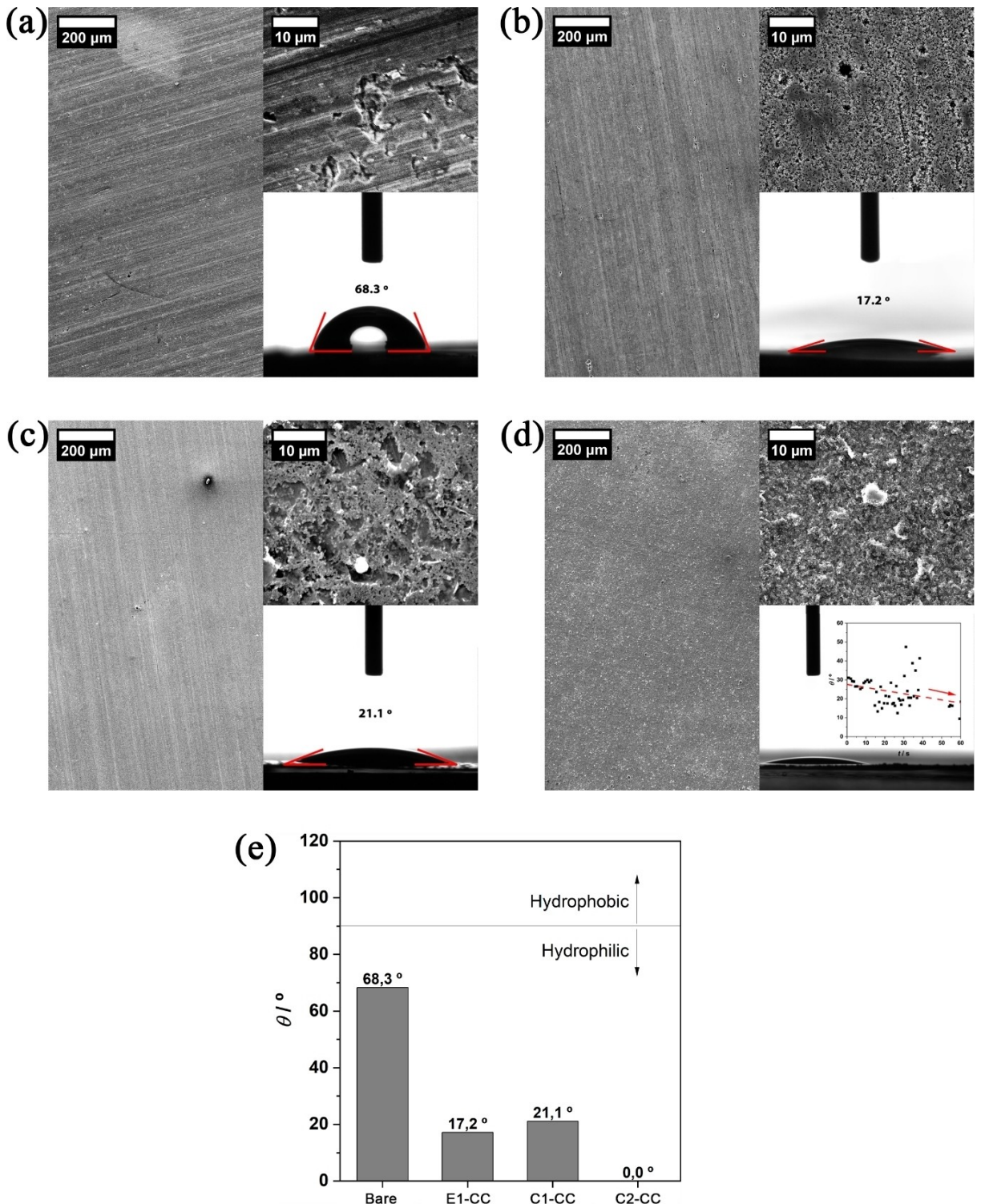


**Figure 1.** Scanning electron micrographs at low and high magnifications and corresponding contact angle measurements on (a) bare, (b) E1-CC, (c) C1-CC and (d) C2-CC, and (e) summary of contact angle values.

size lower than 12 μm could be identified, with carbon black agglomerates filling the interstitial spaces. Moreover, due to the particle morphology of AC, channels were formed, which allow electrolyte permeation into the bulk of the electrode. At a macroscale, no cracks or defects were found; instead, a uniform

electrode film was obtained. The high-quality laminates were achieved by the suitable combination and dispersion of slurry components, which possesses the appropriate rheological properties (Figure S1) for the coating technique adopted, but also a good spreading of the slurry on the aluminium foils,

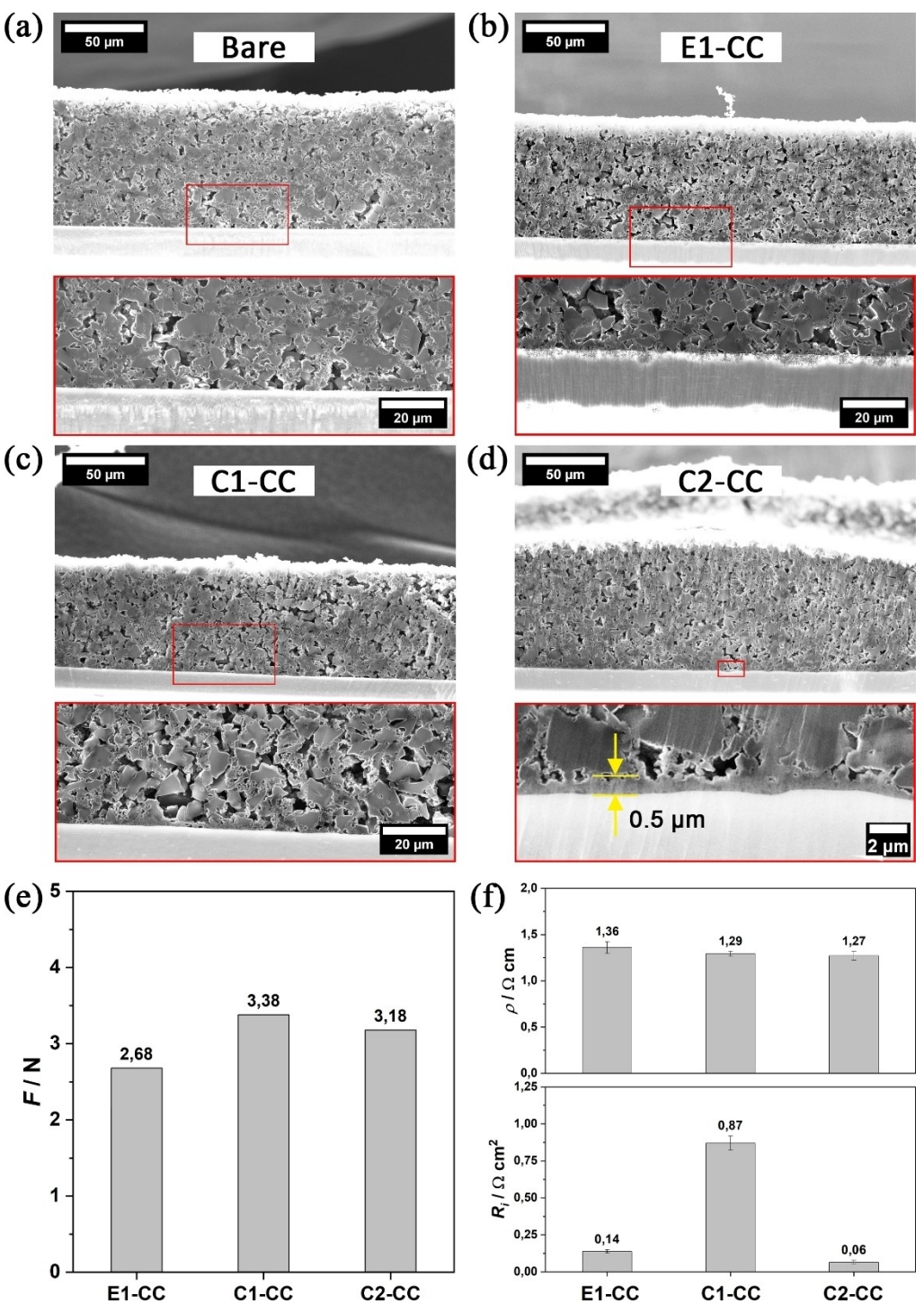


**Figure 2.** Physicochemical properties of laminates. (a-d) Cross-sectional micrographs, (e) peeling force required to detach the coating from the current collector and (f) bulk resistivity of coating on the aluminium current collectors.

which ensures an adequate contact between the coating and the current collector. Further analysis at the interface in Figure 2(b) shows submicrometer-sized pits on the E1-CC (see also Figure 1(b)), which could serve as additional anchoring sites for the coated materials. In Figure 2(c,d) are depicted coatings on carbon-coated aluminium foils. However, a thin and heterogeneous coating could be found on C1-CC (Figure 2(c)).

On the other hand, a firm continuous layer of carbon, with approximately 0.5 μm, could be spotted at the interface between the metallic foil and the coating in C2-CC (Figure 2(d)). The continuous porous carbon coating secures an intimate contact between the coating components and the aluminium foil, providing an efficient electric pathway.

In order to evaluate the mechanical stability of the coating but also the physical binding between the coating components, the adhesive properties were also assessed. Images of the electrodes subjected to the peel test are shown in Figure S2. As reported in Figure 2(e), coatings on C1-CC and C2-CC possess the highest bonding strengths, 3.38 N and 3.18 N, respectively, and E1-CC reports the lowest, 2.68 N. The superior bonding strengths recorded in coated aluminium foils could be attributed to the chemical similarity and compatibility between the carbon-rich slurry components and the carbon layer, as shown in Figure 1(c,d), that facilitate a good interfacial bonding. On the other hand, the pits observed in E1-CC might not possess enough pore width to mechanically interlock the elements of the coating, hence requiring less energy to debond the laminate components. Additionally, the electrical properties were investigated to determine the influence of aluminium modification in the electric conductivity. As shown in Figure 2(f), similar bulk resistivities were recorded for the coatings, ranging between 1.27 and 1.36  $\Omega\text{cm}$ . However, significantly high values of contact resistance were recorded in laminates with C1-CC ( $0.87 \Omega\text{cm}^2$ ), almost an order of magnitude higher compared to laminates with E1-CC ( $0.14 \Omega\text{cm}^2$ ) and C2-CC ( $0.06 \Omega\text{cm}^2$ ) current collector. This could be due to the setup of the multi-point probe that accounts not only the contact resistances between the electrode and the coating, the coating and the current collector, but also the resistance of the coating. As observed in Figure 1(c), the aluminium foil was covered in a thin, non-uniform carbon coating, which could result in the electrical disruption between sections of the conductive coating but also failing to reach an electrical threshold due to localized variations of conductive material. In sum, this would result in higher coating resistance, hence the considerably high contact resistance values reported for C1-CC. On the other hand, the low values of contact resistance observed in both E1-CC and C2-CC further confirm that an effective physical contact was achieved between the electrode and the current collectors, resulting in an efficient electron transfer between the electrically connected elements of the cell.

### 2.3. Electrochemical Characterization

In Figure 3(a–e) are reported CVs of EDLCs with modified aluminium current collector. Rectangular profiles are observed, revealing a purely capacitive charge storing mechanism. In agreement, the charge-discharge profiles in Figure 3(f) also demonstrate a capacitive behavior, described by the linearity and symmetry during charge and discharge. Although similar electrochemical outputs were observed for the investigated electrodes, certain differences were encountered. For instance, E1-CC and C2-CC possess similar areal capacitances while C1-CC reports the lowest. Moreover, C2-CC depicts the best rate capabilities, a property inherently related to the internal resistance. As reported in Figure S3(a), C2-CC possesses the lowest internal resistance,  $1.61 \Omega$ , while E1-CC and C1-CC report  $1.91$  and  $2.42 \Omega$ , respectively. Consequently, the iR drop is more sensitive towards changes of current, as observed in Figure S3

(b). As previously stated, the presence of a homogeneous porous carbon coating in C2-CC provides a high surface of contact towards the coated materials, while the inherent conductive properties of the carbon allow an efficient flow of electrons between the coating and the current collector, resulting in a lower internal resistance. Although E1-CC is characterized by a rough conductive surface, the lack of structural conformity between the micrometer-sized pits and the active material results in a less intimate contact, hence higher internal resistance. In contrast, higher internal resistance was observed in C1-CC, which could be attributed to the considerably lower physical contact between the coating materials and the smooth aluminium surface. Although the modified current collector possesses a thin carbon layer, the conductive particles are heterogeneously distributed on the surface, hindering an efficient electron exchange within the electrode, resulting in higher contact resistance.

The stability encountered throughout the electrochemical studies clearly demonstrates that water-processed electrodes can be used in EDLCs. Beyond that, their use as electrodes in Li-ion and Na-ion chemistries has also been explored targeting the future development of water processed all-carbon metal ion capacitors. Their electrochemical performance in 1 M LiPF<sub>6</sub> (EC:DMC) and in 1 M NaPF<sub>6</sub> (EC:PC) is reported in the supplementary section (Figure S4 and Figure S5). As a main conclusion, water processed electrodes perform well under the abovementioned electrolytes, enabling the possibility to discard the need to employ environmentally noxious fluorine-rich polymers and toxic organic solvents for the development of MICs. Additionally, since the AC electrodes are expected to be employed as positive electrodes, they were characterized in the range 2–4 V vs. M<sup>+</sup>/M (M=Li, Na). As reported, the CVs depict rectangular signals while GCD profiles are described by the linearity and symmetry during charge and discharge, both methods revealing a purely capacitive charge storing mechanism,<sup>[36]</sup> which are in agreement with previously reported results in the literature.<sup>[37–41]</sup>

Back to EDLCs, given the poorer performance of C1-CC, only E1-CC and C2-CC were further investigated as main conductive scaffolds for water-processed electrodes in a monolayer pouch cell configuration. Careful selection of electrodes was conducted, in order to obtain equal mass loadings from pouch cell to pouch cell. Moreover, given the chemical properties of the electrolyte, the mass loading ratio between the positive and negative side was limited to 1.1:1 to achieve a suitable charge balance. The specifications of the pouch cells can be found in Table S1.

The CVs of the pouch cells with E1-CC and C2-CC are reported in Figure 4(a,b) and depict a purely capacitive charge-storing mechanism arising from the rectangularity demonstrated in the profiles for all scan rates tested. Nyquist-represented electrochemical impedance is reported in Figure 4(c), comparing the spectra of E1-CC and C2-CC. As shown, E1-CC depicts higher ESR compared to C2-CC,  $117$  and  $77 \text{ m}\Omega$ , respectively. Galvanostatic charge-discharge profiles are shown in Figure 4(d) performed at 10 A. The profiles are characterized by symmetric triangular signals. Moreover, both E1-CC and C2-

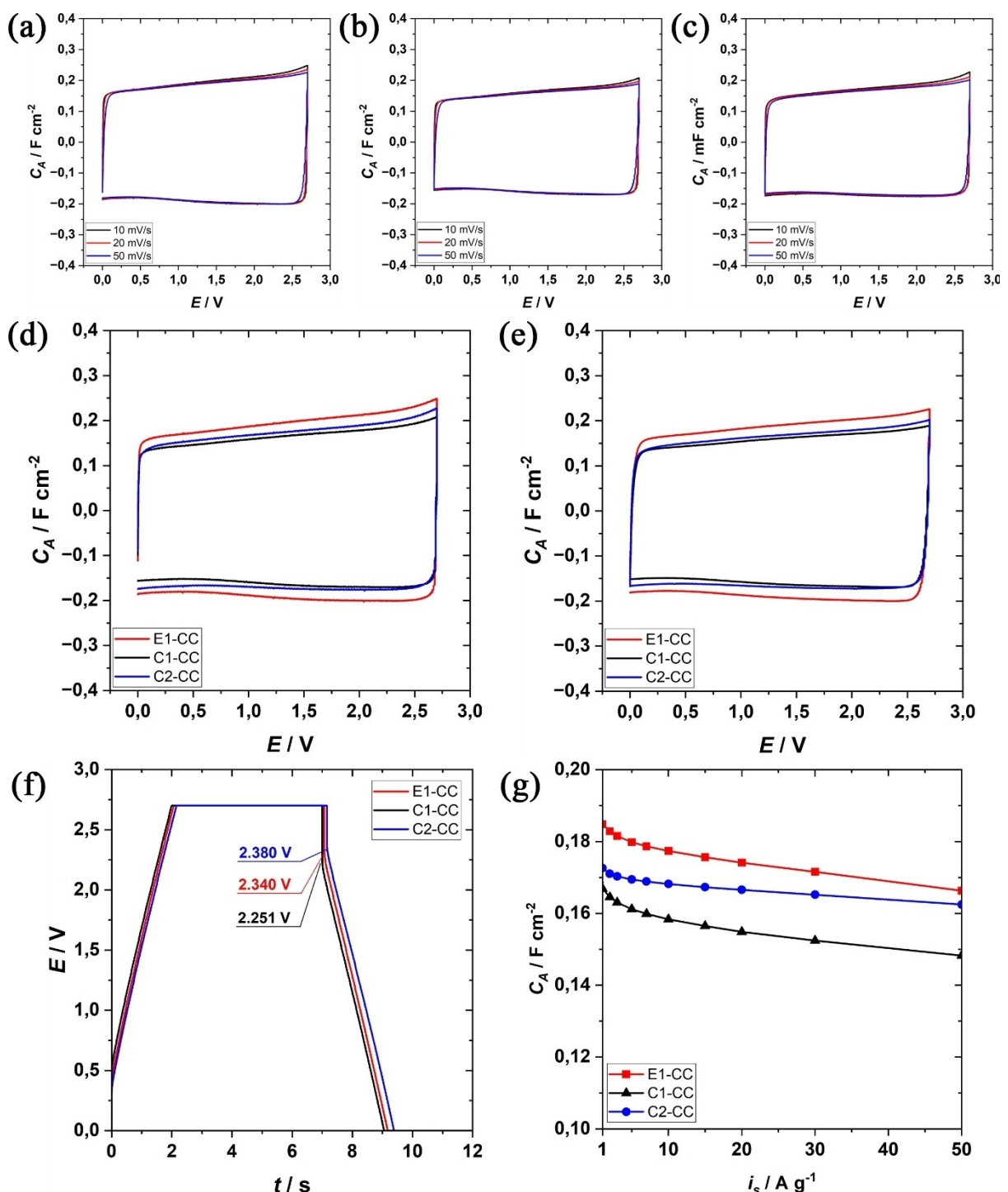


**Figure 3.** Electrochemical investigations of electrodes in different aluminium current collectors. CVs ranging between 10 and 50  $\text{mV s}^{-1}$  in (a) E1-CC, (b) C1-CC and (c) C2-CC. Comparison of voltammograms at (d) 10  $\text{mV s}^{-1}$  and (e) 50  $\text{mV s}^{-1}$ . (f) Charge-discharge profiles at 30  $\text{A g}^{-1}$  and (g) rate capability.

CC depict similar discharge times, while C2-CC reports a lower iR drop, which is in agreement with the electrochemical impedance spectrum (see Figure 4(c)). The lower internal resistance observed in C2-CC, provided by the intimate contact between the coating and the current collector, resulting from the dense homogeneous carbon conductive interlayer, generates additional electrical pathways allowing an efficient collec-

tion of current. On the other hand, the lower contact achieved between the coated particles and the etched pits in E1-CC might be the reason for the higher contact resistance.

Despite the superior electrical properties bestowed by C2-CC, the robustness of the current collector during long-term cyclability and lifespan of the pouch cells has to be considered. Suitable physical contact with the current collector is of utmost

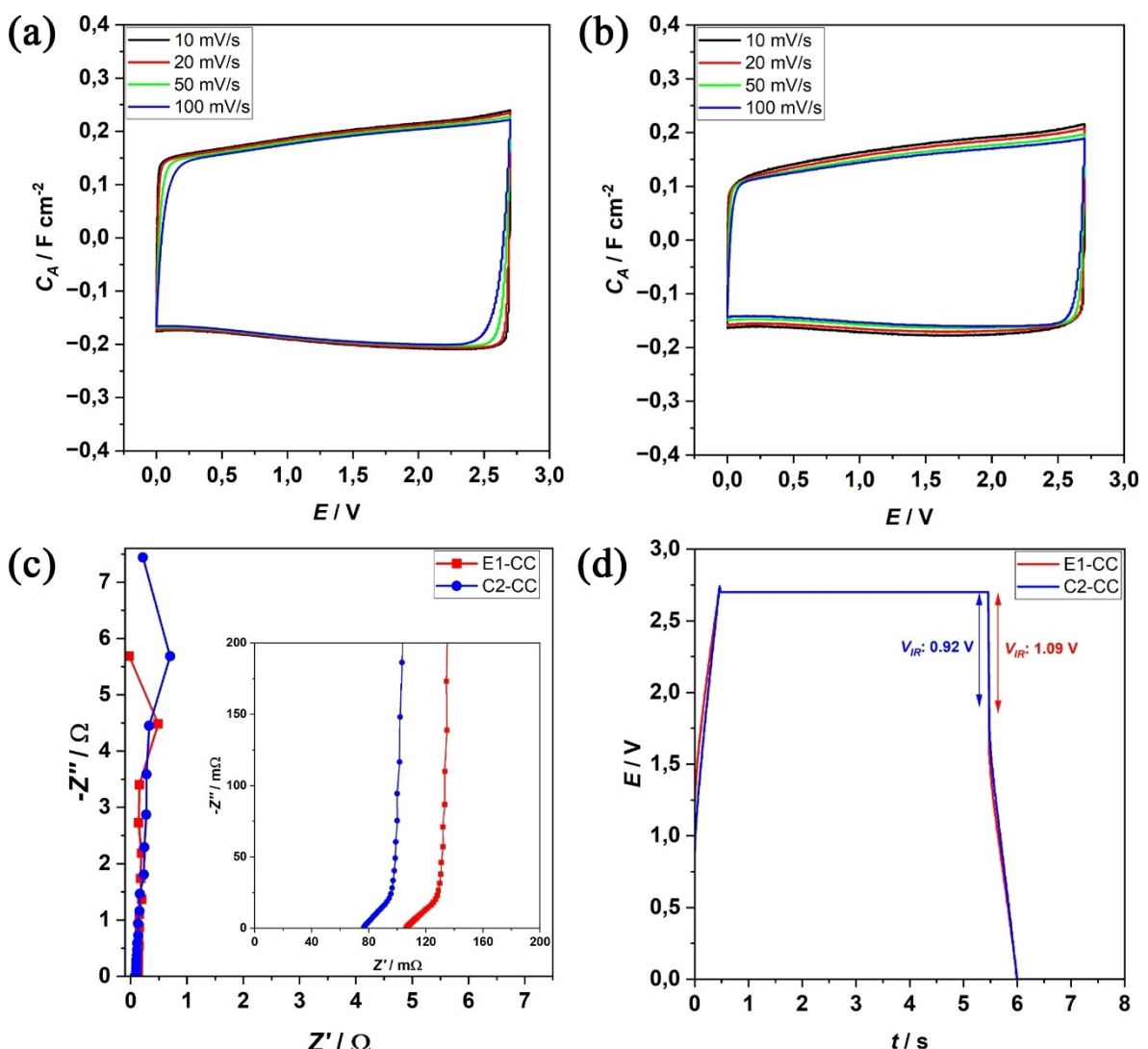


**Figure 4.** Electrochemical investigations of pouch cells. CVs at scan rates ranging between 10 and 100  $\text{mV s}^{-1}$  in (a) E1-CC and (b) C2-CC. (c) Electrochemical impedance spectroscopy analysis. (d) Galvanostatic charge-discharge profiles at 10.0 A ( $62 \text{ Ag}^{-1}$ ).

importance since mechanical failure of the electrode typically occurs at the interphase of the electrode components and can lead to delamination along the phase boundaries. Failure to achieve a reasonable physical and electrical contact between the components can result in a sharp increase of ohmic resistance due to electrical interruption.<sup>[23]</sup> As a consequence, the imminent formation and propagation of microcracks can occur and is further potentiated at high rates due to the localized heat release arising from an irreversible Joule effect, which accelerates solvent evaporation kinetics, promoting gas evolution.<sup>[42,43]</sup> In this sense, a suitable selection of current collector will determine the lifespan of the device.

#### 2.4. Long-Term Cyclability and Post-Mortem Investigations

Ageing studies were performed in order to investigate the impact of the modified aluminium current collectors on the long-term stability and lifetime in pouch cells. Typically, the

degradation of supercapacitors is promoted by applying thousands of galvanostatic charge/discharge cycles at current densities higher than  $1 \text{ A g}^{-1}$ , while monitoring the evolution of internal resistance and nominal capacitance.<sup>[44,45]</sup> A common criterion to determine the end of life is generally set to 20% loss of the nominal capacitance or an increase of 100% of equivalent series resistance. Herein, ageing was accelerated through aggressive conditions, by applying  $30 \text{ A g}^{-1}$  in pouch cells with E1-CC and C2-CC with their nominal capacitance, internal resistance and impedance profiles recorded.

Figure 5(a,b) report the evolution of the electrochemical impedance spectra for both E1-CC and C2-CC for 300,000 cycles. The analysis of the spectra at low frequencies (Figure 5(a)) demonstrates that an increase of the imaginary impedance occurs with ageing regardless of the current collector employed, which is attributed to a decay in the storing properties of the devices. This decay could be attributed to the loss of porosity arising from the formation of a solid interphase due to reactions occurring between the electrolyte and electrode

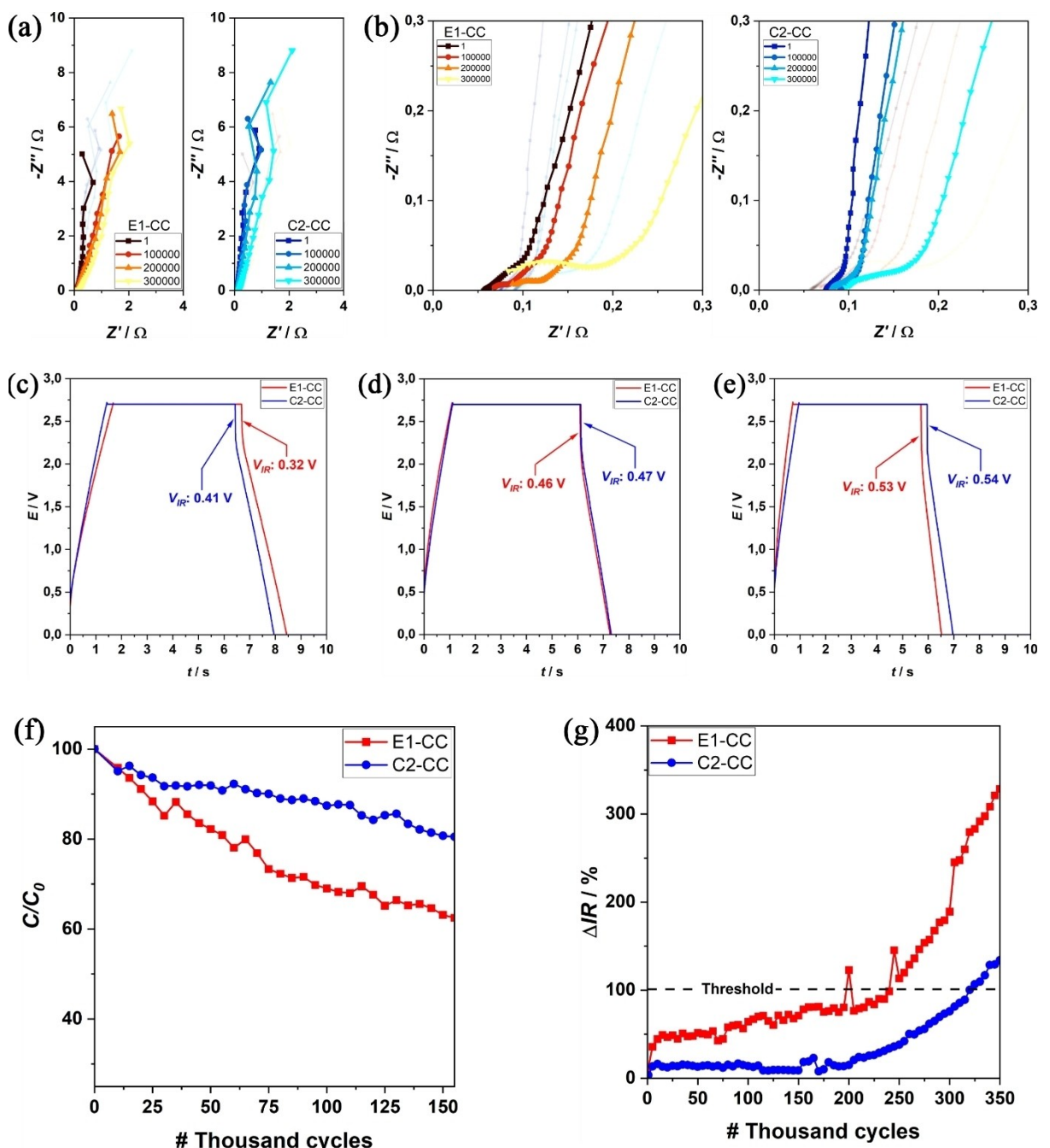


**Figure 5.** Ageing studies of pouch cells. Evolution of the EIS showing the (a) full spectra and focusing at the (b) low frequencies. Galvanostatic charge-discharge profiles in the (c) beginning, after (d) 10,000 cycles and (e) 100,000 cycles. Evolution of (f) nominal capacitance and (g) equivalent series resistance.

active material, parallelly leading to electrolyte starvation.<sup>[46]</sup> In acetonitrile-based EDLCs, the degradation is more pronounced in the positive electrode, which reaches the potential stability limit sooner. Consequently, reactions prone to such potentials occur between the solvent and surface functionalities of the activated carbon, the binder and traces of water if present.<sup>[47]</sup> Additionally, a rapid inclination of the spectra at low frequencies is observed in E1-CC after 100,000 cycles, while a gradual leaning is reported in C2-CC. The decrease of the slope at low frequencies could be interpreted as a shift towards a less ideal-

capacitive behavior, and is better described by a constant phase element, indicating changes in the homogeneity of the electrode surface.<sup>[48]</sup> At high-to-medium frequencies (Figure 5(b)) the spectra of both cells depict a quasi-ideal EDLC, defined by the equivalent series resistance followed by the in-pore resistance region. However, the appearance of a semicircle in E1-CC could be identified between the initial 100,000 cycles, with a progressive increase of its intensity. On the other hand, it is noted that significant changes were reported in C2-CC after 200,000 cycles due to the appearance of two overlapping

semicircles, which could be attributed to the resistive response of passivating coatings developed at the interphases of the electrodes. With regard to the equivalent series resistance, no substantial changes have been observed in the pouch cells. The analysis of the spectra demonstrated that the electrodes are still vulnerable to decay in storing properties. Nevertheless, it is believed that the imminent exposure of the current collector to the electrolyte accelerates performance degradation, as observed by the semicircle in E1-CC. On the other hand, the presence of a carbon layer in C2-CC delayed the ageing process by protecting the current collector. Analysis of the charge-discharge profiles in Figure 5(c-e) supports the abovementioned observations with regards to the robustness of C2-CC towards ageing. Although E1-CC reports slightly higher discharge periods and lower iR drop compared to C2-CC during the initial cycles, the situation rapidly changed after 10,000 cycles, with both cells demonstrating similar electrochemical outputs, while after 100,000 cycles C2-CC outperforms. This is further confirmed through the analysis of Figure 5(f,g). While 80% of the nominal capacitance (Figure 5(f)) is achieved after 145,000 cycles and the equivalent series resistance (Figure 5(g)) doubles after 320,000 cycles in C2-CC, E1-CC reaches the end of life at less cycles. Moreover, E1-CC depicts a sharp increase of equivalent series resistance through the initial 10,000 cycles of approximately 50%, with a gradual increase. By contrast, C2-CC shows an increase of 16% of internal resistance after the initial cycles with a steady value until 200,000 cycles.

Considering the unmatched decay of nominal capacitance and equivalent series resistance (see Figure 5(f,g)), it could be stated that the parameters are not fully interdependent. The degradation of the storing properties is strongly related to the changes occurring at the active material, while the evolution of the equivalent series resistance and appearance of dielectrics relies on the processes that result in the decay of the overall conductive properties of the electrodes. As previously noted, the parameters that mostly contributed to the changes in the EIS are related to the formation and gradual growth of the semicircle and, at a higher degree, the leaning and growth of the spectra at low frequencies. Most likely, this is related to the formation of a passivating layer at the surface of the current collector an increment of the heterogeneity of the electrode surface and a loss of porosity. Accordingly, the quality of the coating strongly influenced the ageing process herein reported. In order to further understand the degree of degradation in the structure of the electrodes, SEM analysis was performed to the aged coatings and current collectors. For comparison, pristine electrodes were also included in the analysis.

Figure 6(a) depicts micrographs of the positive electrode materials before and after ageing. Compared to the pristine electrode, deposits could be identified at the surface of E1-CC and C2-CC, possibly from the reaction with the electrolyte's solvent. This is further supported by the presence of fluorine signals in the aged electrodes, arising from fluoride composition products.<sup>[47]</sup> The formation of deposits would explain the decrease in storing properties of the pouch cells, which limit the accessibility of the ionic charge carriers to the electroactive surface of the activated carbon. Analysis of cross-sectioned

aged E1-CC in Figure 6(b) depicts a brittle coating with poor cohesion that easily detached from the current collector. As previously mentioned, intimate contact between the current collector and the coating is required not only to minimize the contact resistance, but also to cease any detrimental reactions at the interphase that could trigger the formation of micro-cracks. Although carbon particles were found bonded to the etched current collector, the delamination of the coating from the current collector evidences the degradation at the interphase, possibly due to the formation of cracks. On the other hand, as observed in Figure 6(c), aged C2-CC possessed enough mechanical strength during handling and demonstrates good interparticle integrity. In Figure 6(c,d) are depicted etched and carbon coated pristine and aged positive aluminium current collectors, respectively. With respect to E1-CC, significant changes occurred after ageing (Figure 6(c)), as depicted by the appearance of newly formed pits and the growth of existing ones, suggesting that leaching occurred at the current collector, possibly from the reaction between HF and aluminium.<sup>[49]</sup> Additionally, the increase of fluorine signals suggests that a solid interphase was formed at the current collector. On the other hand, the surface of C2-CC after ageing demonstrates no visible topological changes. Moreover, no fluorine signals were detected before and after ageing, implying that the carbon coating protected the aluminium against degradation reactions. The presence of Na signals in all the samples analyzed could be ascribed to the CMC.

XRD investigations performed on pristine and aged positive aluminium current collectors of E1-CC and C2-CC (Figure S6) demonstrate defined aluminium signals ( $45.3^\circ$ ,  $65.1^\circ$  and  $78.3^\circ$ ) in all samples, while the decrease of intensity in some of Al signals together with very low intensity signals of what might be  $\text{AlF}_3$  at  $21.5^\circ$ ,  $\text{Al}_2\text{O}_3$  at  $36^\circ$  and  $70^\circ$ , and  $\text{AlBO}_3$  at  $45^\circ$  are described after ageing, suggesting that decomposition reactions occurred at the interface between the aluminium current collector and the coated materials. Additional NMR investigations were conducted into the electrolyte of aged pouch cells (see Figure S7).  $^{19}\text{F}$  NMR experiments in Figure S7a and S7b describe  $\text{BF}_4^-$  in the chemical shift at around  $-151.9$  ppm. Meanwhile, the shift at  $-194.7$  ppm describes the presence of tetrafluoroaluminate ( $\text{AlF}_4^-$ ) in E1-CC (see Figure S7c), while in C2-CC the compound was not found.  $^{27}\text{Al}$  NMR signals at  $49.71$ – $48.74$  ppm in Figure S7d confirm the presence of  $\text{AlF}_4^-$ . The formation of  $\text{AlF}_4^-$  occurs from the reaction between aluminium and corrosive HF, with the latest produced from electrochemically driven reactions between functionalities at the surface of the activated carbon or water present in the system.<sup>[49]</sup> The detection of HF in E1-CC supports the previous claim that leaching occurred at the surface of etched aluminium current collector, hence the substantial topological alterations compared to its pristine counterpart. Moreover, the structural decay of the coating in E1-CC could be explained from decomposition reactions occurring between HF and the binder. On the other hand, the absence of  $\text{AlF}_4^-$  in C2-CC suggests that the formation reaction of HF has not occurred with intensities comparable to E1-CC. As a result, the electrodes in C2-CC preserved their initial structure as noticed in Figure 6(c,e).

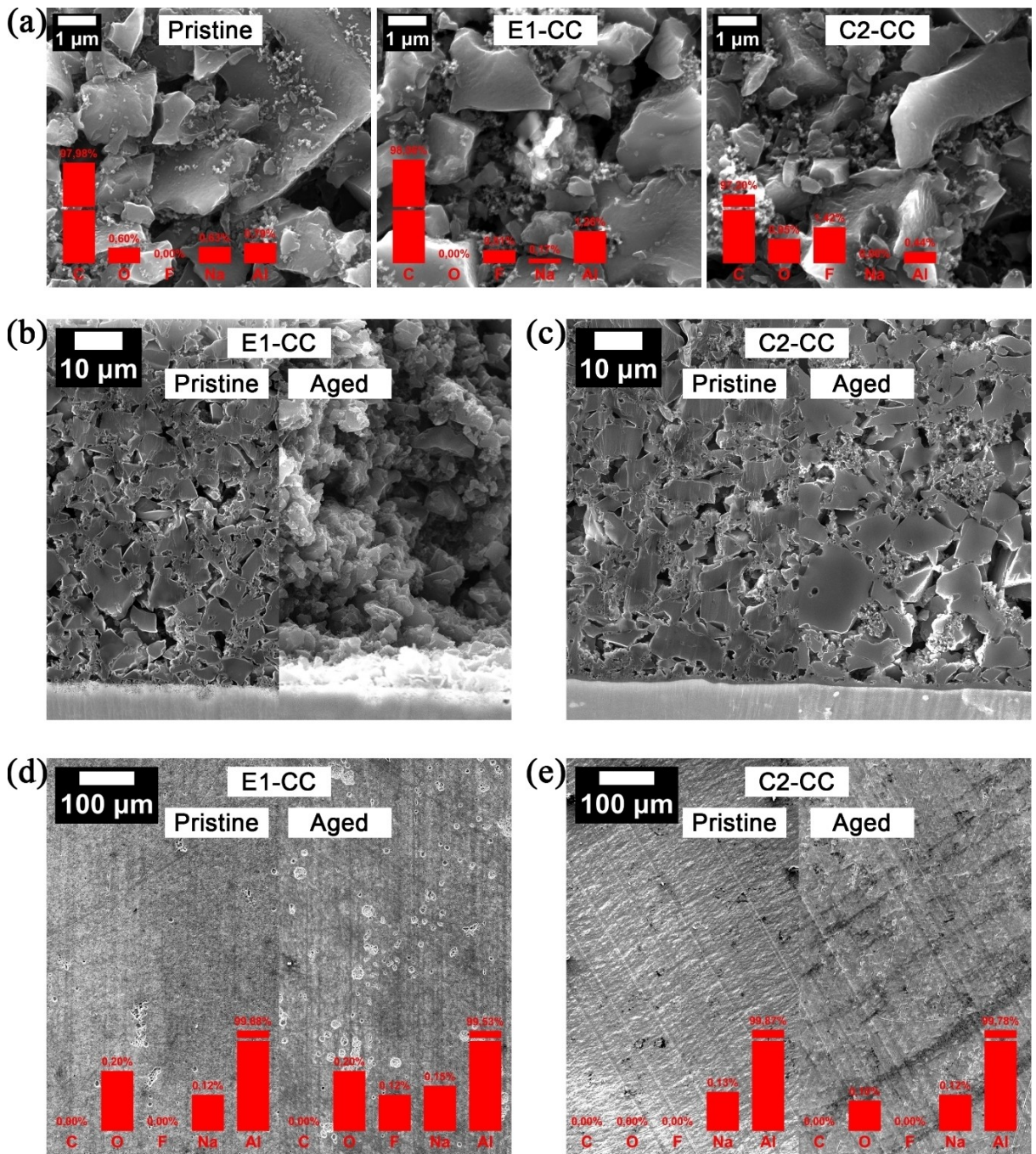


**Figure 6.** Post-mortem investigations. (a) Microstructural analysis of the electrodes materials before cycling (left), aged E1-CC (middle) and C2-CC (right). Cross-sectional micrographs of pristine and aged (b) E1-CC and (c) C2-CC electrodes. Pristine and aged current collector (d) E1-CC and (e) C2-CC.

These observations are consistent with the EIS (see Figure 5(b)), where a growing semicircle was found in the aged spectra of E1-CC, which is related to the deterioration of the contact resistance. In contrast, C2-CC depicts depressed semicircles with a lower intensity, suggesting lower contact resistances between the coating and the current collector. As previously discussed, it is believed that the carbon coating in C2-CC acts as an electrically conductive barrier that physically hampers the contact of the electrolyte with the aluminium while allowing the efficient exchange of current between the

electrode components. On the other hand, the exposed surface of the etched aluminium accelerates the decomposition of the electrolyte, resulting in the deterioration of the interface in the long-term. Moreover, this could be further potentiated by the unmatching active material particle size and pit dimensions, which generates a significantly wider open surface for detrimental reactions to occur.

The study indicates that the current collector is prone to detrimental reactions which impart the overall performance of the device. However, modifications at the interface through

etching or carbon priming of aluminium foil significantly improved the wetting properties, resulting in electrodes with suitable mechanical properties and low ESRs. It was also shown that the presence of a continuous conductive carbon coating was found to profoundly affect the electrochemical performance, as noted by lower internal resistances which resulted in superior rate capabilities, ascribed to an intimate contact between the electrode elements through the conductive interlayer, allowing an efficient flow of electrical charge carriers. Moreover, the coating also functions as a physical barrier between the coating and the current collector, slowing the ageing of the device. On the other hand, the morphological mismatch between the coated materials and the etched pits results in higher contact resistances, delivering poorer performance while promoting reactions that cause microcracks and electrolyte decomposition. This degradation not only causes solvent depletion but also deteriorates the binder of the coating. In contrast, the presence of a thick and homogeneous carbon coating reduces the contact with the electrolyte and the current collector, retarding possible degradation reactions. Additionally, the low contact resistance provided by the conductive carbon further reduces the likelihood of microcrack-forming reactions. In summary, among the analyzed current collectors, uniformly carbon-coated current collectors emerged as the optimal choice, outperforming other studied current collectors.

### 3. Conclusions

In summary, utilization of surface-modified current collectors was found beneficial in maximizing the physicochemical properties of water-processed activated carbon electrodes. Manufactured laminates in both etched and carbon-coated aluminium foils were crack-free and possessed suitable adhesion. Electrochemically, the electrodes demonstrated similar performances, hence validating their use in different chemistries. Further investigations in pouch cells also portrayed similar performances. Nonetheless, higher rate capabilities were found in electrodes employing carbon-coated aluminium current collector, likely due to the intimate contact between the electrode and the carbon coating, leading to lower interfacial resistance. Additionally, ageing and post-mortem investigations demonstrated that the carbon coating served as a protective layer towards detrimental reactions that could impart the long-term cyclability of the electrochemical energy storing devices.

### Acknowledgements

Authors would like to acknowledge The MUSIC project, funded by the European Union's Horizon Europe research and innovation programme under grant agreement number 101092080; and the Basque Government for the ELKARTEK 2023 call (project CICe2023) under the application number KK-2023/00063.

### Conflict of Interests

The authors declare no conflict of interest.

### Data Availability Statement

The data that support the findings of this study are available from the corresponding author upon reasonable request.

**Keywords:** Current collector · Aluminium · Activated carbon · High-power · Electrochemical capacitor

- [1] "RMIS - Critical, strategic and advanced materials," can be found under <https://rmis.jrc.ec.europa.eu/eu-critical-raw-materials>, n.d.
- [2] G. G. Amatucci, F. Badway, A. Du Pasquier, T. Zheng, *J. Electrochem. Soc.* **2001**, *148*, A930.
- [3] M. Arnaiz, J. L. Gómez-Cámer, E. Gonzalo, N. E. Drewett, J. Ajuria, E. Goikolea, M. Galceran, T. Rojo, *Mater. Today Proc.* **2021**, *39*, 1118–1131.
- [4] D. Bresser, D. Buchholz, A. Moretti, A. Varzi, S. Passerini, *Energy Environ. Sci.* **2018**, *11*, 3096–3127.
- [5] D. L. Wood, J. D. Quass, J. Li, S. Ahmed, D. Ventola, C. Daniel, *Dry. Technol.* **2018**, *36*, 234–244.
- [6] D. Bresser, D. Buchholz, A. Moretti, A. Varzi, S. Passerini, *Energy Environ. Sci.* **2018**, *11*, 3096–3127.
- [7] P. Ruschhaupt, A. Varzi, S. Passerini, *ChemSusChem.* **2020**, *13*, 763–770.
- [8] A. Varzi, A. Balducci, S. Passerini, *J. Electrochem. Soc.* **2014**, *161*, A368–A375.
- [9] N. Böckenfeld, S. S. Jeong, M. Winter, S. Passerini, A. Balducci, *J. Power Sources* **2013**, *221*, 14–20.
- [10] L. Köps, P. Ruschhaupt, C. Guhrenz, P. Schlee, S. Pohlmann, A. Varzi, S. Passerini, A. Balducci, *J. Power Sources* **2023**, *571*, 233016.
- [11] C. Schütter, S. Pohlmann, A. Balducci, *Adv. Energy Mater.* **2019**, *9*, 1900334.
- [12] H. Jeong, J. Jang, C. Jo, *Chem. Eng. J.* **2022**, *446*, 136860.
- [13] A. Abdissattar, M. Yeleuov, C. Daulbayev, K. Askaruly, A. Tolynbekov, A. Taurbekov, N. Prikhodko, *Electrochim. Commun.* **2022**, *142*, 107373.
- [14] C. Vaalma, D. Buchholz, M. Weil, S. Passerini, *Nat. Rev. Mater.* **2018**, *3*, 1–11.
- [15] A. Abdissattar, M. Yeleuov, C. Daulbayev, K. Askaruly, A. Tolynbekov, A. Taurbekov, N. Prikhodko, *Electrochim. commun.* **2022**, *142*, 107373.
- [16] H. Nara, D. Mukoyama, R. Shimizu, T. Momma, T. Osaka, *J. Power Sources* **2019**, *409*, 139–147.
- [17] D. Y. Shin, D. H. Park, H. J. Ahn, *Appl. Surf. Sci.* **2019**, *475*, 519–523.
- [18] N. Issatayev, A. Nuspeissova, G. Kalimuldina, Z. Bakenov, *J. Power Sources Adv.* **2021**, *10*, 100065.
- [19] D. Y. Shin, D. H. Park, H. J. Ahn, *Appl. Surf. Sci.* **2019**, *475*, 519–523.
- [20] M. M. Loghavi, M. Askari, M. Babaiee, A. Ghasemi, *J. Electroanal. Chem.* **2019**, *841*, 107–110.
- [21] T. Hang, H. Nara, T. Yokoshima, T. Momma, T. Osaka, *J. Power Sources* **2013**, *222*, 503–509.
- [22] L. Romoli, A. H. A. Lutey, G. Lazzini, *CIRP Annals* **2022**, *71*, 481–484.
- [23] C. Zwahr, N. Serey, L. Nitschke, C. Bischoff, U. Rädel, A. Meyer, P. Zhu, W. Pfleging, *Int. J. Extreme Manuf.* **2023**, *5*, 035006.
- [24] W. Dong, K. Wang, J. Han, Y. Yu, G. Liu, C. Li, P. Tong, W. Li, C. Yang, Z. Lu, *ACS Appl. Mater. Interfaces* **2021**, *13*, 8417–8425.
- [25] S. H. Wang, Y. X. Yin, T. T. Zuo, W. Dong, J. Y. Li, J. L. Shi, C. H. Zhang, N. W. Li, C. J. Li, Y. G. Guo, *Adv. Mater.* **2017**, *29*, 1703729.
- [26] S. Lee, E. S. Oh, *J. Power Sources* **2013**, *244*, 721–725.
- [27] J. H. Park, J. Ku, J. W. Lim, J. M. Choi, I. H. Son, *J. Electroanal. Chem.* **2016**, *778*, 53–56.
- [28] C. Busson, M. A. Blin, P. Guichard, P. Soudan, O. Crosnier, D. Guyomard, B. Lestriez, *J. Power Sources* **2018**, *406*, 7–17.
- [29] M. Onsrud, A. O. Tezel, S. Fotedar, A. M. Svensson, *SN Appl. Sci.* **2022**, *4*, 1–7.
- [30] D. Y. Semerukhin, A. V. Kubarkov, E. V. Antipov, V. G. Sergeyev, *Mendeleyev Commun.* **2023**, *33*, 206–208.
- [31] P. Luis, D. Southee, G. W. Weaver, U. Wijayantha, *Flex. Print. Electron.* **2023**, *8*, 025007.

- [32] T. Li, H. Bo, H. Cao, Y. Lai, Y. Liu, *Int. J. Electrochem. Sci.* **2017**, *12*, 3099–3108.
- [33] A. Ojstrsek, O. Plohl, S. Gorgjeva, M. Kurecic, U. Janicic, S. Hribenik, D. Fakin, *Sensors* **2021**, *21*, 3508.
- [34] S. Krainer, U. Hirn, *Colloids Surf. A Physicochem. Eng. Asp.* **2021**, *619*, 126503.
- [35] R. N. Wenzel, *Ind. Eng. Chem.* **1936**, *28*, 988–994.
- [36] M. Hahn, M. Baertschi, O. Barbieri, J. C. Sauter, R. Kotz, R. Gallay, *J. Solid State Chem.* **2004**, *7*, A33.
- [37] S. R. Sivakkumar, A. G. Pandolfo, *Electrochim. Acta* **2012**, *65*, 280–287.
- [38] W. J. Cao, J. P. Zheng, *J. Power Sources* **2012**, *213*, 180–185.
- [39] T. Panja, J. Ajuria, N. Díez, D. Bhattacharjya, E. Goikolea, D. Carriazo, *Scientific Reports* **2020**, *10*, 1–11.
- [40] J. Ajuria, E. Redondo, M. Arnaiz, R. Mysyk, T. Rojo, E. Goikolea, *J. Power Sources* **2017**, *359*, 17–26.
- [41] S. Jayaraman, A. Jain, M. Ulaganathan, E. Edison, M. P. Srinivasan, R. Balasubramanian, V. Aravindan, S. Madhavi, *Chem. Eng. J.* **2017**, *316*, 506–513.
- [42] A. Bothe, A. Balducci, *J. Power. Sources* **2022**, *548*, 232090.
- [43] S. Ishimoto, Y. Asakawa, M. Shinya, K. Naoi, *J. Electrochem. Soc.* **2009**, *156*, A563.
- [44] E. Pameté, L. Köps, F. A. Kreth, S. Pohlmann, A. Varzi, T. Brousse, A. Balducci, V. Presser, *Adv. Energy Mater.* **2023**, *13*, 2301008.
- [45] A. Burke, M. Miller, *Electrochim. Acta* **2010**, *55*, 7538–7548.
- [46] P. W. Ruch, D. Cericola, A. Foelske-Schmitz, R. Kotz, A. Wokaun, *Electrochim. Acta* **2010**, *55*, 4412–4420.
- [47] F. A. Kreth, L. H. Hess, A. Balducci, *Energy Storage Mater.* **2023**, *56*, 192–204.
- [48] R. Kotz, P. W. Ruch, D. Cericola, *J. Power Sources* **2010**, *195*, 923–928.
- [49] K. Chiba, T. Ueda, Y. Yamaguchi, Y. Oki, F. Shimodate, K. Naoi, *J. Electrochem. Soc.* **2011**, *158*, A872.

Manuscript received: June 21, 2024

Revised manuscript received: July 23, 2024

Accepted manuscript online: July 26, 2024

Version of record online: September 17, 2024